Springer

Journal of Mechanical Science and Technology 23 (2009) 578~589

Journal of
Mechanical
Science and
Technology

www.springerlink.com/content/1738-494x
DOI 10.1007/s12206-008-1001-9

Laminar flow past a sphere rotating in the transverse direction †

Dongjoo Kim*

School of Mechanical Engineering, Kumoh National Institute of Technology, Gumi, Gyeongbuk 730-701, Korea

(Manuscript Received August 7, 2008; Revised October 8, 2008; Accepted October 8, 2008)

Abstract

Laminar flow past a sphere rotating in the transverse direction is numerically investigated in order to understand the effect of the rotation on the characteristics of flow over the sphere. Numerical simulations are performed at Re = 100, 250 and 300, where the Reynolds number is based on the free-stream velocity and the sphere diameter. The rotational speeds considered are in the range of $0 \le \omega^* \le 1.2$, where ω^* is the maximum velocity on the sphere surface normalized by the free-stream velocity. Without rotation, the flow past a sphere experiences steady axisymmetry, steady planar-symmetry, and unsteady planar-symmetry, respectively, at Re = 100, 250 and 300. With rotation, however, the flow becomes planar-symmetric for all the cases investigated, and the symmetry plane of flow is orthogonal to the rotational direction. Also, the rotation affects the flow unsteadiness, and its effect depends on the rotational speed and the Reynolds number. The flow is steady irrespective of the rotational speed at Re = 100, whereas at Re = 250 and 300 it undergoes a sequence of transitions between steady and unsteady flows with increasing ω^*. As a result, the characteristics of vortex shedding and vortical structures in the wake are significantly modified by the rotation at Re = 250 and 300. For example, at Re = 300, vortex shedding occurs at low values of ω^*, but it is completely suppressed at $\omega^* = 0.4$ and 0.6. Interestingly, at $\omega^* = 1$ and 1.2, unsteady vortices are newly generated in the wake due to the shear layer instability. The critical rotational speed, at which the shear layer instability begins to occur, is shown to be higher at Re = 250 than at Re = 300.

Keywords: Sphere; Wake; Transverse rotation; Vortex shedding; Shear layer instability

1. Introduction

Flow over a rotating sphere is of interest in many engineering applications associated with particle transport because solid particles, which are generally modeled as spheres, in a flow translate and rotate simultaneously due to particle-particle or particle-wall collisions. Therefore, it is important to understand the effect of rotation on the flow over a rotating sphere. However, only a little knowledge has been obtained for the characteristics of flow over a rotating sphere, and this is particularly because previous studies mainly focused on the force applied on the sphere with relatively little attention to flow characteristics. Another reason is that flow over a sphere shows completely unsteady three-dimensional phenomena even at low Reynolds number.

The characteristics of flow over a rotating sphere depend significantly on the direction of rotation. One important direction of rotation is the streamwise direction, where the rotational direction is the same as that of translation. This rotation is equivalent to the revolution of axisymmetric bodies such as a bullet. The other direction is the transverse one, where the direction of rotation is orthogonal to that of translation. Note that the flow over a transversely rotating sphere corresponds to the three-dimensional counterpart of flow over a circular cylinder rotating about the cylinder axis.

For streamwise rotation, there have been several studies published in the literature and some important flow

† This paper was recommended for publication in revised form by Associate Editor Dongshin Shin

* Corresponding author. Tel.: +82 54 478 7301, Fax.: +82 54 478 7319
E-mail address: kdj@kumoh.ac.kr

characteristics have been revealed. For example, Schlichting [1] summarized previous results on flow over a streamwisely rotating sphere and introduced two specific features. First, the drag and the critical Reynolds number, at which the drag coefficient decreases abruptly, depend strongly on the rotational speed [2]. Second, the line of separation is moved upstream due to the rotation [3]. Recently, Kim & Choi [4] numerically investigated the effect of the streamwise rotation on the drag, lift and vortical structures of laminar flow over a sphere up to Re = 300. In their study, the authors found an interesting flow phenomenon called 'frozen', where the vortical structures in the wake simply rotate without temporal variation in their strength.

On the other hand, for transverse rotation, which is of the present interest, quite a few studies have been conducted mainly focusing on the relation between the rotational speed and the force (especially the lift known as Magnus effect) exerted on the sphere. For very low Reynolds numbers, Rubinow & Keller [5] derived a correlation between the rotational speed and the force on the sphere by using matched asymptotic expansions. The derived correlation shows that the rotation does not affect the drag, whereas the lift increases with the rotational speed. The lift by Rubinow & Keller [5] may be written in a non-dimensional form as $C_l = 2\omega^*$. Here, C_l is the lift coefficient and $\omega^* (= \omega R / u_\infty)$ is the non-dimensional rotational speed, where ω is the angular velocity of the sphere, R is the radius of the sphere, and u_∞ is the freestream velocity. On the other hand, at Reynolds numbers greater than unity, the lift coefficient does not follow the relation derived by Rubinow & Keller [5] but it depends on the Reynolds number and the rotational speed. For example, Barkla & Auchterlonie [6] experimentally obtained the relation of $C_l = (0.16 \pm 0.04)\omega^*$ for $1500 < \mathrm{Re} < 3000$ and $2 < \omega^* < 4$, while Tsuji et al. [7] reported $C_l = (0.40 \pm 0.10)\omega^*$ for $150 < \mathrm{Re} < 1600$ and $\omega^* < 0.7$. Later, Oesterlé & Dinh [8] found from their experimental study that C_l increases with increasing ω^* or decreasing Re and proposed a relation for the range of $10 < \mathrm{Re} < 140$ and $1 < \omega^* < 6$. However, the dependency of C_l on Re becomes smaller with increasing Reynolds number, and C_l is almost independent of Re at high Reynolds numbers ($\mathrm{Re} > 10^4$), as explained by Oesterlé & Dinh [8].

Despite many previous studies, only little knowledge has been obtained for the moderate Reynolds number range ($100 \le \mathrm{Re} \le 300$) of the present interest. Furthermore, to the best of the author's knowledge, there has been little effort to investigate the effect of the transverse rotation on the characteristics of three-dimensional flow behind the sphere except the following recent studies. Kurose & Komori [9] numerically investigated the flow over a rotating sphere ($1 \le \mathrm{Re} \le 500$, $0 \le \omega^* \le 0.25$) in a linear shear flow and found that the vortex shedding frequency increases with increasing rotational speed or fluid shear rate. Meanwhile, Niazmand & Renksizbulut [10] numerically examined the effects of the sphere rotation and the surface blowing on wake structure for $0 \le \omega^* \le 1$ at $\mathrm{Re} \le 200$ and $0 \le \omega^* \le 0.5$ at $200 < \mathrm{Re} \le 300$. They found that the rotation causes vortex shedding to occur at lower Reynolds numbers (e.g., $\mathrm{Re} = 200$ at $\omega^* = 0.5$) as compared to the case of a non-rotating sphere. These studies revealed some important aspects of the flow characteristics, but their results are limited to relatively low rotational speeds.

One of the interesting issues is whether or not the rotation of the sphere can suppress vortex shedding from the sphere. In case of the flow over a circular cylinder, i.e., the two-dimensional counterpart of the present study, some researchers [11, 12] reported that vortex shedding is completely suppressed by the rotation of the cylinder at relatively high rotational speeds. Also, Mittal & Kumar [12] found that the flow becomes unsteady again at very high rotational speeds. Interestingly, the suppression of vortex shedding (at $\omega^* = 0.4$ and 0.6) and reappearance of unsteady flow (at $\omega^* = 1$) were also found in the sphere wake at Re = 300 in the author's preliminary study [13]. Therefore, one of the objectives of this paper is to understand the underlying physics for these phenomena with an in-depth discussion. In this study, numerical simulations are performed in order to investigate the effect of the transverse rotation on three-dimensional vortical structures of flow over a sphere. In addition, the variations of the Strouhal number, drag and lift forces due to the rotation are also investigated in detail. For these purposes, the Reynolds number and the rotational speed have been carefully chosen in this study. The Reynolds numbers considered are 100, 250 and 300 covering steady axisymmetric, steady planar-symmetric and unsteady planar-symmetric flows without rotation. The non-dimensional rotational speed ω^* is in the range of $0 \le \omega^* \le 1.2$, which is wide enough to resolve the above-mentioned issue as will be explained below.

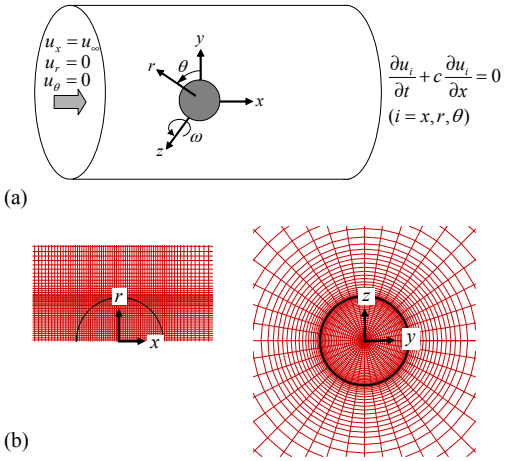

Fig. 1. (a) Coordinate system and boundary conditions; (b) mesh near the sphere.

2. Numerical details

In the present study, flow over a sphere is simulated in a cylindrical coordinate system by using an immersed boundary method [14]. In this method, momentum forcing and mass source/sink are introduced inside the sphere to satisfy the no-slip condition on the sphere surface and the continuity for the cells containing the immersed boundary, respectively. This method has been successfully applied to various laminar and turbulent flows: for example, laminar flows over a sphere and a hemisphere [4, 15, 16] and turbulent flow over a sphere [17, 18]. For the details of the present numerical method, see Kim et al. [14] and Kim & Choi [4].

Fig. 1 shows the coordinate system, computational domain and mesh near the sphere. As explained before, the cylindrical coordinate system is employed, where x, r and θ denote the streamwise, radial and azimuthal directions, respectively. A Cartesian coordinate system (x, y, z) is also defined in order to represent the drag and lift forces, where the lift force is decomposed into two orthogonal (y and z) components. The computational domain used is $-15d \le x \le 15d$, $0 \le r \le 15d$ and $0 \le \theta < 2\pi$, where ($x = 0$, $r = 0$) corresponds to the center location of the sphere and d is the sphere diameter. A Dirichlet boundary condition ($u_x = u_\infty$, $u_r = 0$, $u_\theta = 0$) is used at the inflow and far-field boundaries, and a convective boundary condition ($\partial u_i / \partial t + c \partial u_i / \partial x = 0$) is used for the outflow boundary, where c is the space-averaged streamwise velocity at the exit. For all the Reynolds numbers, a non-uniform mesh is used with dense resolution at $r \cong 0.5d$ for accurately capturing the separating shear layer around the sphere. The number of grid points used is $385(x) \times 131(r) \times 40(\theta)$. The number of grid points and the computational domain size were carefully determined from an investigation of their effect on the solution. In the case of rotating sphere, the direction of the rotation coincides with the $z-$axis, i.e., orthogonal to the streamwise direction as shown in Fig. 1(a), and the non-dimensional rotational speed investigated is $0 \le \omega^* (= \omega R / u_\infty) \le 1.2$. In the present study, flows past a stationary sphere are first simulated and then they are used as initial flow fields when flows past a rotating sphere are simulated.

Table 1. Simulation results for flow over a stationary sphere. Here, $\overline{C_d}$ and $\overline{C_l}$ are the time-averaged drag and lift coefficients, respectively.

	Re	$\overline{C_d}$	$\overline{C_l}$	St
Present	100	1.087		
	250	0.702	0.061	
	300	0.658	0.067	0.134
Fornberg [19]	100	1.085		
Johnson & Patel [20]	250	0.70	0.062	
	300	0.656	0.069	0.137
Constantinescu & Squires [21]	250	0.70	0.062	
	300	0.655	0.065	0.136
Tomboulides & Orszag [22]	300	0.671		0.136

Table 1 shows the present results for flow over a stationary sphere together with those from previous numerical studies [19-22] in which body-fitted grids were used. Here, flows at Re = 100, 250 and 300 represent three different laminar flow regimes: steady axisymmetric flow ($\mathrm{Re} \le 200$), steady planar-symmetric flow ($210 \le \mathrm{Re} \le 270$), and unsteady planar-symmetric flow ($280 \le \mathrm{Re} < 375$) [20,22-24]. As clearly shown in Table 1, the drag and lift coefficients, and the Strouhal number ($St = fd / u_\infty$), where f is the vortex shedding frequency, are all in good agreement with the previous results.

3. Results

3.1 Vortical structure

Fig. 2 shows the variation of vortical structures with the rotation at Re = 100, where the surfaces of vortical structures are identified by using the method of Jeong & Hussain [25]. When the sphere is stationary ($\omega^* = 0$), the flow is steady axisymmetric and no

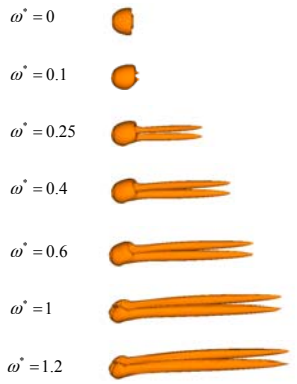

Fig. 2. Variation of vortical structures with the rotational speed at Re = 100.

vortical structure exists in the wake. On the other hand, in the case of rotating sphere ($\omega^* > 0$), a non-axisymmetric velocity field is induced by the transverse rotation of the sphere and the flow becomes steady planar-symmetric, losing axisymmetry. As a result, a pair of vortical structures are generated behind the rotating sphere for $\omega^* \geq 0.25$. With increasing rotational speed, these structures become stronger and elongated in the streamwise direction. Note that the vortical structures at $\omega^* \geq 0.25$ (especially, at $\omega^* = 0.25$) are very similar to those of the flow past a stationary sphere at Re = 250 (see the case of $\omega^* = 0$ in Fig. 4).

To understand the effect of rotation on the velocity field, the streamlines near the sphere are shown on the (x, y)- and (x, z)-planes for various rotational speeds at Re = 100 in Fig. 3. As the rotational speed increases, the upward deflection (i.e., in the $+y$ direction) of the wake becomes significant (see left figures) and the recirculation region behind the sphere becomes smaller at $\omega^* = 0.25$ and eventually disappears at $\omega^* = 0.6$ (see right figures). This observation is in good agreement with the numerical results of Niazmand & Renksizbulut [10] where the recirculation region ceases to exist for $\omega^* \geq 0.5$. It is also clear from this figure that the flow over a rotating sphere is planar-symmetric and the symmetry plane is the (x, y)-plane, i.e., orthogonal to the rotational axis ($z-$axis). This feature is also true for the two other Reynolds numbers considered in this study.

Fig. 4 shows the variation of vortical structures with rotation at Re = 250. Without rotation, the flow is steady planar-symmetric and a pair of streamwise vortices appear in the wake. At $\omega^* = 0.1$, the vortices become stronger due to the rotation as at Re = 100, but they are periodically split into two parts and convect downstream, resulting in unsteady wake. The unsteadiness due to the rotation becomes significant at $\omega^* = 0.25$, and vortex shedding occurs in the form of hairpin vortex which is similar to the vortex in the unsteady flow past a stationary sphere at Re = 300 (see Fig. 5). However, at larger rotational speeds ($\omega^* = 0.4$, 0.6, and 1), vortex shedding is completely suppressed and thus the flow returns to a steady state. In this range of ω^* showing steady flow, there is little variation in vortical structures and their common feature is that a pair of vortical structures in the wake are elongated down to the exit boundary. On the other hand, at $\omega^* = 1.2$, the flow becomes unsteady again and periodic vortex loops are generated in the wake. The occurrence of unsteady vortex loops at high rotational speeds is also found at Re = 300 as explained below and further discussion will be made in § 3.2.

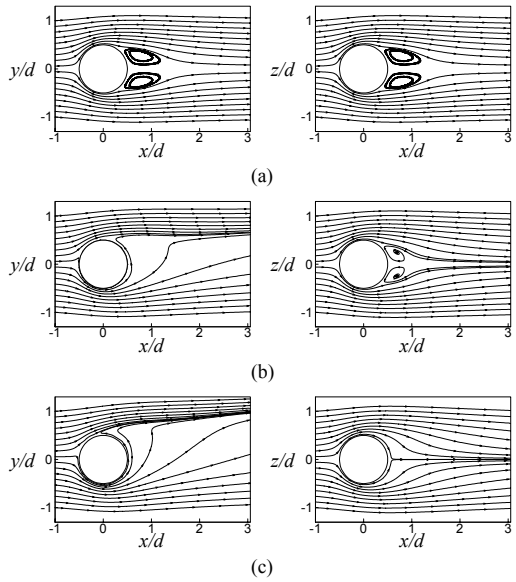

Fig. 3. Streamlines on the (x, y)- and (x, z)-planes at Re = 100: (a) $\omega^* = 0$; (b) $\omega^* = 0.25$; (c) $\omega^* = 0.6$.

Fig. 5 shows the variation of vortical structures with the rotation at Re = 300. For a stationary sphere, the flow is unsteady planar-symmetric due to the periodic shedding of hairpin vortices maintaining planar-symmetry. At low rotational speeds ($0 \leq \omega^* \leq 0.25$), there is no significant change in vortical structures except that the distance between consecutive vortices decreases due to the increase of the vortex shedding frequency with increasing rotational speed. On the

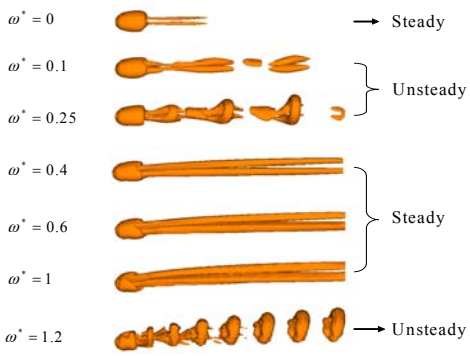

Fig. 4. Variation of vortical structures with the rotational speed at Re = 250.

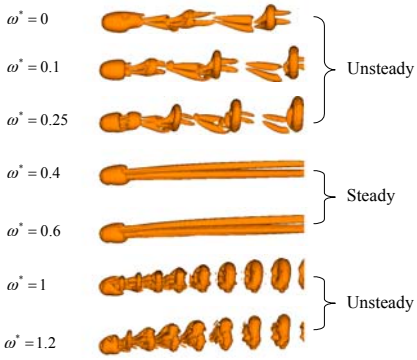

Fig. 5. Variation of vortical structures with the rotational speed at Re = 300.

other hand, at intermediate rotational speeds ($\omega^* = 0.4$ and 0.6), vortex shedding is completely suppressed as in the case of Re = 250. It is very interesting to note that a similar phenomenon was also observed in the flow past a rotating circular cylinder by some researchers [11,12]. For example, Kang et al. [11] numerically found that for a given Reynolds number at which vortex shedding occurs from a stationary cylinder, the flow over a rotating cylinder maintains vortex shedding at low rotational speeds but vortex shedding completely disappears at rotational speeds higher than the critical value (e.g., $\omega^*_{crit} = 1.8$ at Re = 100).

The suppression of vortex shedding from a sphere observed at $\omega^* = 0.4$ and 0.6 for Re = 300, however, is not maintained at higher rotational speeds (Fig. 5). That is, the flow becomes unsteady again at $\omega^* = 1$ and 1.2, similar to the case of $\omega^* = 1.2$ at Re = 250 (Fig. 4). Therefore, it is clear that there are two separate unsteady flow regimes for both Reynolds numbers, but the critical rotational speed for the occurrence of the second unsteady regime is lower at Re = 300 ($0.6 < \omega^*_{crit} \le 1$). A close look at Fig. 5 shows that wake structures in the second unsteady regime at high rotation speeds ($\omega^* = 1$ and 1.2) are quite different from those in the first unsteady regime at low rotational speeds ($0 \le \omega^* \le 0.25$). First, shed vortices take the form of a hairpin vortex composed of the head and legs at $0 \le \omega^* \le 0.25$, whereas at $\omega^* = 1$ and 1.2, the strength of the legs is weak and thus vortices manifest themselves in vortex loops as they convect downstream. Second, the vortex shedding frequencies at $\omega^* = 1$ and 1.2 are much higher than those in the range of $0 \le \omega^* \le 0.25$ (see Fig. 14 for quantitative analysis). Note that a similar reappearance of unsteady flow at very high rotational speeds was also observed in the flow over a rotating cylinder by Mittal & Kumar [12]. They found that vortex shedding observed for $\omega^* < 1.91$ is suppressed for $1.91 \le \omega^* \le 4.34$, but unsteady flow appears again in the range of $4.34 < \omega^* < 4.70$.

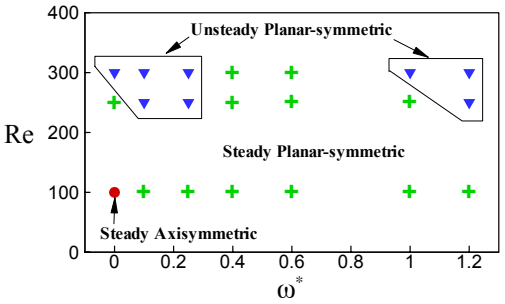

Fig. 6. Flow regimes depending on the Reynolds number and the rotational speed. ●, steady axisymmetric flow; +, steady planar-symmetric flow; ▼, unsteady planar-symmetric flow.

To summarize the findings, the flows over a sphere with and without the transverse rotation can be categorized into three different flow regimes depending on the Reynolds number and the rotational speed as shown in Fig. 6. The flow regimes are steady axisymmetric, steady planar-symmetric, and unsteady planar-symmetric flows. From the viewpoint of unsteadiness, the flow at Re = 100 is steady for all the rotational speeds investigated, whereas at Re = 250 and 300, the flows experience a series of transitions between steady and unsteady flows depending on the rotational speed. However, in terms of flow symmetry, flow over a rotating sphere is planar-symmetric for all the cases investigated.

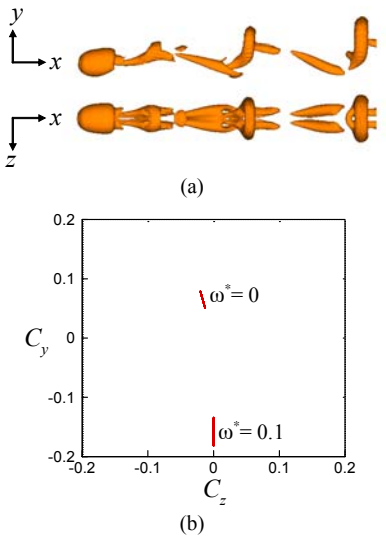

Fig. 7. Vortical structures and phase diagram for Re = 300 and $\omega^* = 0.1$: (a) instantaneous vortical structures with rotation; (b) phase diagram of the lift coefficients (C_y , C_z).

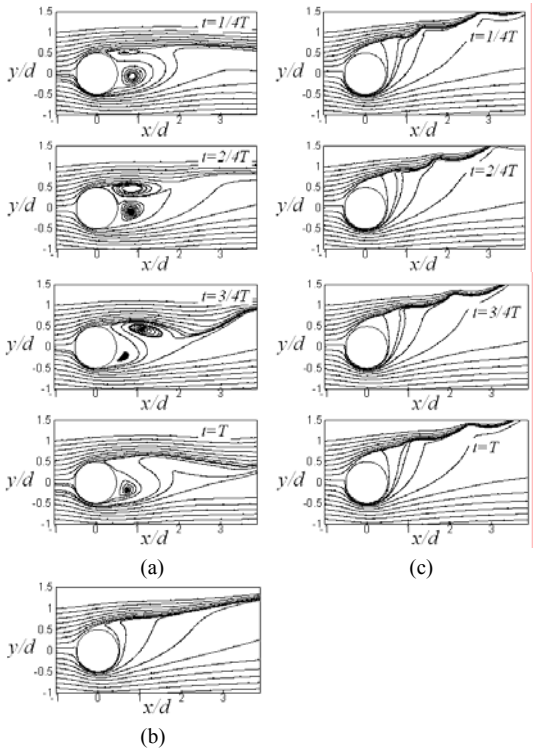

Fig. 8. Streamlines on the (x, y)-plane at Re = 300: (a) $\omega^* = 0.1$; (b) $\omega^* = 0.6$; (c) $\omega^* = 1$. In case of unsteady flow, the time sequence of streamlines is shown during one period (T).

It should be noted here that there is a difference in the direction of flow symmetry between the planar-symmetric flows with and without rotation. In the case of stationary sphere ($\omega^* = 0$), the location where the vortex loop is detached is *a priori* unknown and determined by numerical disturbances such as round-off errors and random disturbances in the initial condition [22]. On the other hand, in the case of rotating sphere ($0.1 \le \omega^* \le 1.2$ in this study), the vortex generation or detachment location is determined by the direction of sphere rotation, so the plane of symmetry becomes the (x, y)-plane as shown in Fig. 7. In the figure, C_y and C_z are the components of lift coefficient in the y and z directions, respectively. Therefore, C_z is zero all the time at $\omega^* = 0.1$, but it is not necessarily zero at $\omega^* = 0$, even though both flows are planar-symmetric. Also, C_y is always negative at $\omega^* = 0.1$ because the direction of the lift force on the sphere is not alternating but fixed in time.

3.2 The second instability at high rotational speeds

As explained before, in the cases of Re = 250 and 300, the flows over a rotating sphere experience a sequence of flow transitions with increasing rotational speed. As a result, there exist two separate unsteady flow regimes, one of which is found at low rotational speeds but the other at high rotational speeds. Based on the observation that the two unsteady flow regimes have different vortical structures and vortex shedding frequency as explained in § 3.1, it may be conjectured that they have different instability mechanisms. At this point, it is reasonable to ask why the flow becomes unsteady again at high rotational speeds. Therefore, in this section, the dynamic characteristics of the two unsteady flow regimes are compared and a possible explanation is suggested for the reappearance of unsteady flow at high rotational speeds.

Fig. 8 shows the streamlines near the sphere on the (x, y) -plane at Re = 300 for various rotational speeds, where the time sequence of streamlines is shown during one period (T) in the case of unsteady flow. In the unsteady flow at $\omega^* = 0.1$ (Fig. 8a), the slow rotation of the sphere does not have much effect on the vortex shedding pattern. At $t = 1/4T$, a vortex is newly formed near the upper shear layer, which entrains fluid from the lower side of the sphere. As time goes on, this vortex grows in strength by entraining fluid from the upper freestream as well as from the lower side of the sphere ($t = 2/4T$), and then it convects downstream forming a limit cycle ($t = 3/4T$).

Finally, the vortical structure loses its spiral appearance ($t = T$), completing one cycle of vortex shedding. This overall procedure is similar to the vortex shedding process from a stationary sphere (see Fig. 25 of Johnson & Patel [20]) except that the vortical structure in the lower side becomes weaker due to the rotation. On the other hand, at $\omega^* = 0.6$ where the flow is steady (Fig. 8b), there exists no vortex behind the sphere due to the enhanced upward motion of the fluid from the lower side. Instead, a thin and stable shear layer is formed at the interface where the upper freestream and the flow entrained from the lower side of the sphere meet together. The stability of the upper shear layer, however, is not maintained at high rotational speeds. At $\omega^* = 1$, where the flow becomes unsteady again (Fig. 8c), the streamlines clearly show an unsteady flow motion in the form of a traveling wave in the upper shear layer. This flow pattern of traveling wave is very different from that with vortex shedding at $\omega^* = 0.1$ (Fig. 8a), and the unsteady flow at $\omega^* = 1$ appears to be triggered not by vortex shedding but by the shear layer instability.

To understand the shear layer characteristics at $\omega^* = 1$ in more detail, azimuthal vorticity contours and particle tracing results are investigated. Fig. 9 shows instantaneous contours of azimuthal vorticity on the (x, y)-plane at $\omega^* = 1$ together with those at $\omega^* = 0.6$ for comparison. At $\omega^* = 0.6$, where the flow is steady (Fig. 9a), the transverse rotation causes the upper shear layer to be elongated to the far downstream region without losing its stability. On the other hand, in the case of unsteady flow at $\omega^* = 1$ (Fig. 9b), the vorticity contours clearly show the existence of shear layer instability at $x > d$. The shear layer characteristics at $\omega^* = 1$ are also examined by performing particle tracking simulation as shown in Fig. 10. Here, at every third computational time step, twenty particles are released uniformly along the radial direction in both the upper ($0.55 \le y/d \le 2$) and lower ($-2 \le y/d \le -0.55$) sides of the sphere at $x = 0.5d$. Fig. 10 corresponds to the snapshot at $t = 16d/u_\infty$ after releasing the particles. The periodic swirling motion of the particles is clearly shown along the upper shear layer, confirming the existence of the shear layer instability.

3.3 Strouhal number and drag and lift coefficients

Fig. 11 shows the time history of drag and lift coefficients at Re = 250, where $C_d (= C_x)$ is the drag coefficient, the lift coefficient $C_l (= \sqrt{C_y^2 + C_z^2})$ denotes the lift magnitude, and C_y and C_z are the components of C_l in the y and z directions, respectively. Note that in the case of rotating sphere, C_l is the same as $-C_y$ because the flow is planar-symmetric ($C_z = 0$) and the lift force is always applied in the $-y$ direction as shown in Fig. 7. As expected from vortical structures in Fig. 4, the drag and lift coefficients are constant in time at $0.4 \le \omega^* \le 1$ where the flow is steady, whereas they are time-periodic in unsteady flow at $\omega^* = 0.1$, 0.25, and 1.2. At $\omega^* = 0.1$ with vortex shedding in the form of streamwise vortices, the fluctuation of lift coefficient is notable but that of drag coefficient is negligible. However, in the case of $\omega^* = 0.25$, hairpin vortices are shed and thus both the drag and lift coefficients clearly show a periodic variation, and their fluctuation amplitudes become larger than those at $\omega^* = 0.1$. Meanwhile, at $\omega^* = 1.2$ where vortex loops are generated due to the shear layer instability, the amplitude of drag fluctuation is larger than that of lift fluctuation.

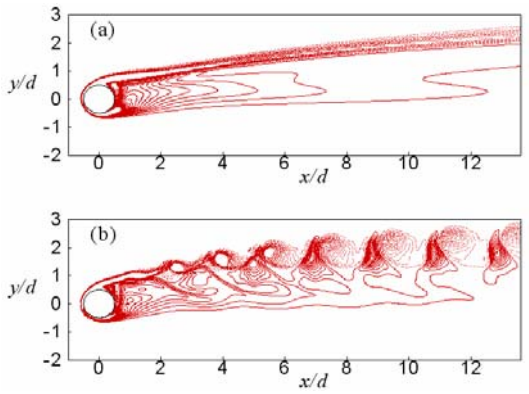

Fig. 9. Contours of azimuthal vorticity on the (x, y)-plane at Re = 300: (a) $\omega^* = 0.6$; (b) $\omega^* = 1$.

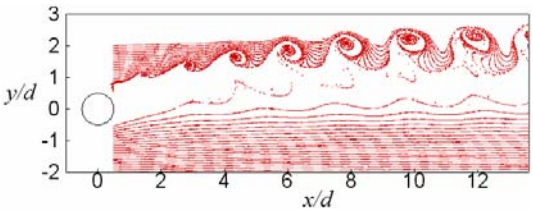

Fig. 10. Flow structure characterized by particle tracing for Re = 300 and $\omega^* = 1$.

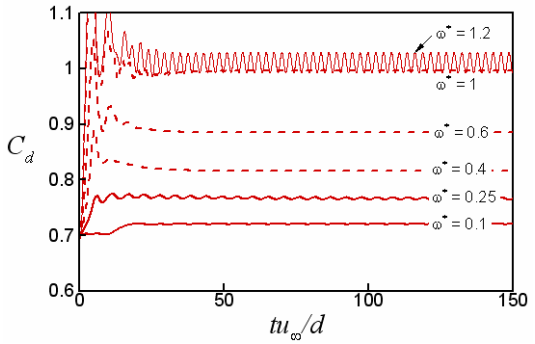

(a)

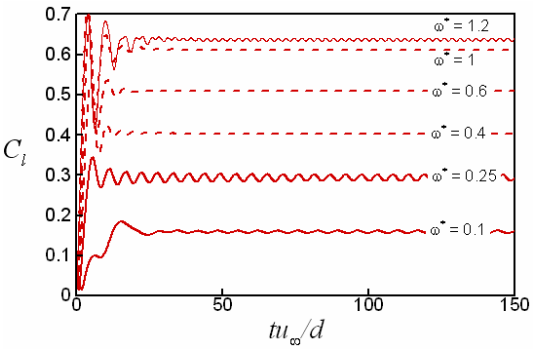

(b)

Fig. 11. Time history of drag and lift coefficients at Re = 250: (a) drag; (b) lift. Solid and dashed lines are used for unsteady and steady flows, respectively. C_d and C_l for $\omega^* = 1$ are denoted by a thick line for a clear comparison with those for $\omega^* = 1.2$.

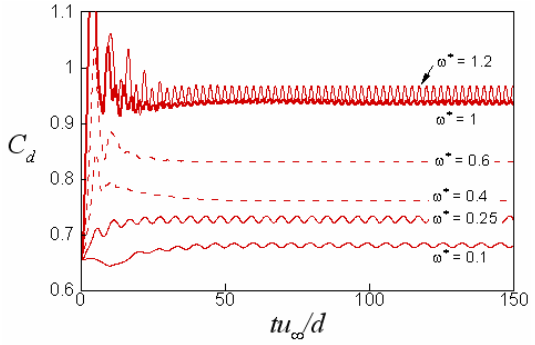

(a)

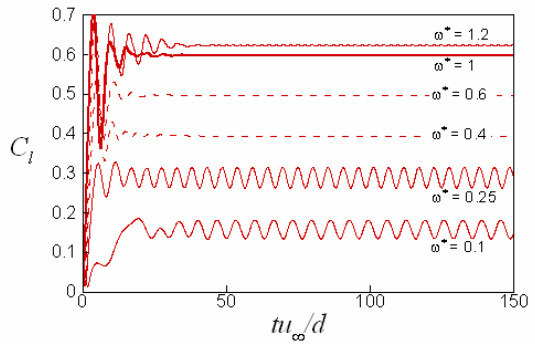

(b)

Fig. 12. Time history of drag and lift coefficients at Re = 300: (a) drag; (b) lift. Solid and dashed lines are used for unsteady and steady flows, respectively. C_d and C_l for $\omega^* = 1$ are denoted by a thick line for a clear comparison with those for $\omega^* = 1.2$.

Observation of unsteady flow for some rotational speeds at Re = 250, where the flow is steady without rotation, implies that the rotation of the sphere triggers instability at a lower Reynolds number. The early instability due to the rotation was also found in the numerical study of Niazmand & Renksizbulut [10], who obtained unsteady flows at Re = 250 in the cases of $\omega^* = 0.16$, 0.25, and 0.5. However, they did not observe the following transitions (returning to steady flow and subsequent second instability) found in this study, because their interest was restricted to the range of $\omega^* \le 0.5$.

Fig. 12 shows the time history of drag and lift coefficients at Re = 300, where hairpin vortices are shed from a stationary sphere (see Fig. 5). At $\omega^* = 0.1$ and 0.25 maintaining the vortex shedding of hairpin vortices, the time-periodic behavior is clearly shown in the drag and lift coefficients. Due to higher vortical strength compared with the vortical structures at Re = 250, the amplitudes of the drag and lift fluctuations at Re = 300 are larger than those at Re = 250, respectively. However, at $\omega^* = 0.4$ and 0.6, the drag and lift coefficients are constant in time due to the suppression of vortex shedding, similar to the case of Re = 250. Finally, at $\omega^* = 1$ and 1.2 showing the instability in the form of vortex loops, the drag coefficient becomes periodic again, but the temporal variation of lift coefficient is negligible.

The dynamic behaviors of the drag and lift forces at Re = 250 and 300 are replotted in the form of phase diagram (C_l, C_d) in Fig. 13. The phase diagram takes the form of a closed curve for time-periodic unsteady flows, but it falls on a point for steady flows. The position of the curve indicates the time-averaged values of C_d and C_l, and its size represents the fluctuation amplitudes. Therefore, it is clear that for both Reynolds numbers the time-averaged values of C_d and C_l monotonically increase with increasing rotational speed, whereas their fluctuation amplitudes show a non-monotonic behavior. That is, the fluctua-

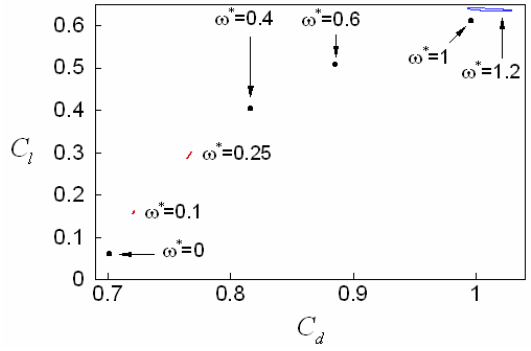

(a)

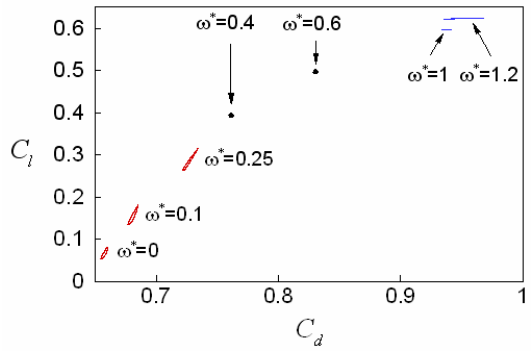

(b)

Fig. 13. Phase diagram of C_l and C_d: (a) Re = 250; (b) Re = 300. Note that the scales of $x-$ and $y-$axes are different.

tion amplitudes of C_d and C_l first increase with increasing rotational speed, but they vanish when the flow is steady. With a further increase in the rotational speed, the fluctuation amplitude of C_d increases again significantly but that of C_l is relatively small (at Re = 250) or negligible (at Re = 300). As a result, at Re = 300, the phase diagrams of high rotational speeds ($\omega^* = 1$ and 1.2) become nearly horizontal lines, which are very different from those of low rotational speeds ($0 \le \omega^* \le 0.25$). This difference between the low and high rotational speed regions may be attributed to the different vortical structures (Fig. 5).

Fig. 14 shows the effect of the rotation on the Strouhal number ($St = fd/u_\infty$), where f is the frequency associated with vortex shedding or shear layer instability. In the present study, the Strouhal number is obtained from the time histories of C_d and C_l. The Strouhal number is zero for steady flow because C_d and C_l are constant. For both Reynolds numbers of 250 and 300, non-zero Strouhal numbers are found in two separate regions, one of

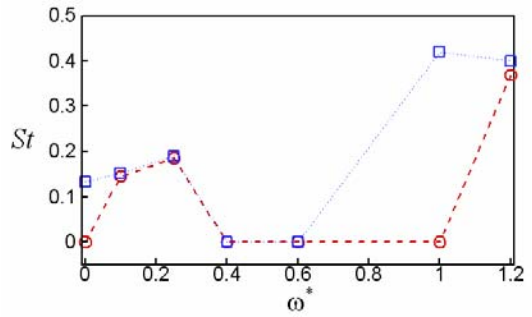

Fig. 14. Effect of the rotation on the Strouhal number ($St = fd/u_\infty$). – – – –, Re = 250; · · · · · ·, Re = 300.

which exists at low rotational speeds ($\omega^* = 0.1$ and 0.25 for Re = 250; $0 \le \omega^* \le 0.25$ for Re = 300) and the other at high rotational speeds ($\omega^* = 1.2$ for Re = 250; $\omega^* = 1$ and 1.2 for Re = 300). In the low ω^* unsteady region, the Strouhal number at Re = 300 increases gradually from the value without rotation ($St = 0.134$) as ω^* increases. This trend is in good agreement with the numerical results by Kurose & Komori [9]. Also, it is clear that for $\omega^* = 0.1$ and 0.25, the effect of the Reynolds number on the Strouhal number is very small between Re = 250 and Re = 300. On the other hand, in the high ω^* unsteady region, the Strouhal number shows a sudden increase due to the shear layer instability with its value being approximately three times greater than that due to vortex shedding at Re = 300 and $\omega^* = 0$.

Fig. 15 shows the variation of the drag and lift coefficients with respect to the rotational speed, where the drag and lift coefficients are averaged over a vortex shedding period in the case of unsteady flow. For comparison, the figure includes the data from Kurose & Komori [9] and Oesterlé & Dinh [8], where C_l values of Oesterlé & Dinh [8] are obtained from the correlation proposed for $10 < \mathrm{Re} < 140$ and $1 \le \omega^* \le 4$. Both the present drag and lift coefficients are in good agreement with the previous results even though the present lift coefficients at Re = 100 are a little larger than the previous ones. For a given Reynolds number, the drag and lift coefficients monotonically increase with the rotational speed. On the other hand, when a rotational speed is fixed, the drag coefficient monotonically decreases with the Reynolds number, whereas the lift coefficient shows a different behavior depending on the rotational speed. That is, with increasing Reynolds number from 100 to 250, the lift coefficient increases if $\omega^* < 0.4$ but it decreases if $\omega^* > 0.4$. However, there exists only a

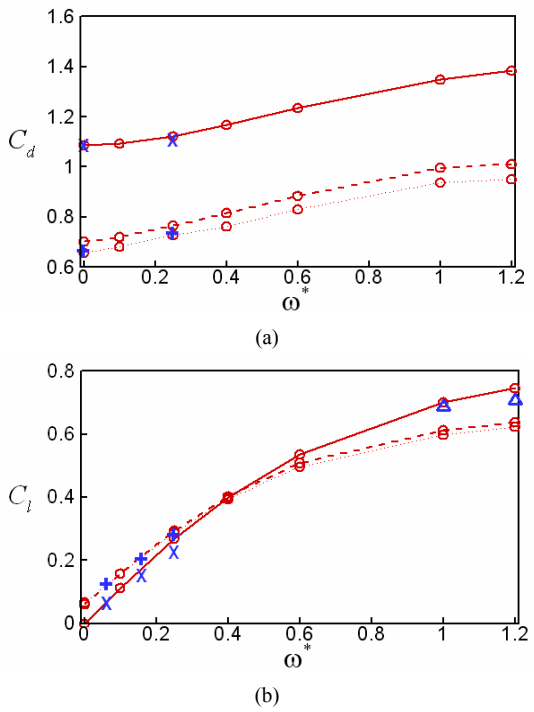

Fig. 15. Variation of drag and lift coefficients with respect to the rotation speed: (a) drag; (b) lift. ———, Re = 100 (present); – – – – –, Re = 250 (present); · · · · · ·, Re = 300 (present); ×, Re=100 (Kurose & Komori [9]); +, Re = 300 (Kurose & Komori [9]); △, Re = 100 (Oesterlé & Dinh [8]).

little variation in C_l between Re = 250 and Re = 300 and this agrees well with the observation made by Kurose & Komori [9] that C_l tends to approach a constant value at high Reynolds numbers ($\mathrm{Re} > 200$).

To explain the variation of the lift force, several researchers have used the ratio of the lift coefficient to the rotational speed (i.e., C_l/ω^*). The ratio C_l/ω^* obtained from the present results is illustrated as a function of ω^* in Fig. 16. For all the Reynolds numbers investigated, the ratio decreases with increasing rotational speed. This trend agrees well with the experimental results of Barkla & Auchterlonie [6] and Oesterlé & Dinh [8]. For the present range of Re and ω^*, the ratio varies between 0.5 and 1.6, which is smaller than the value of two derived by Rubinow & Keller [5] for very low Reynolds number.

4. Summary and concluding remarks

Laminar flow past a sphere rotating in the transverse direction was simulated by using an immersed boundary method in order to investigate the effect of the rotation on the vortical structures behind the sphere as well as the drag and lift forces exerted on the sphere. Numerical simulations were performed at Re = 100, 250 and 300 in the range of $0 \le \omega^* \le 1.2$. The results showed that the flow around the sphere strongly depends on both the Reynolds number and the rotational speed.

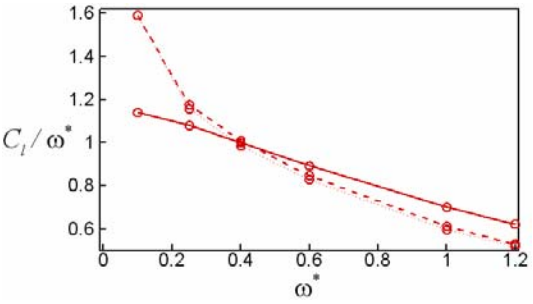

Fig. 16. Variation of C_l/ω^* with respect to the rotational speed. ———, Re = 100; – – – – –, Re = 250; · · · · · ·, Re = 300.

The flows over a sphere with and without the transverse rotation were categorized into three different flow regimes: steady axisymmetric, steady planar-symmetric and unsteady planar-symmetric flows. At $\omega^* = 0$ (without rotation), the flow past the sphere was steady axisymmetric, steady planar-symmetric, and unsteady planar-symmetric at Re = 100, 250 and 300, respectively. With the transverse rotation, the flow became planar-symmetric for all the cases investigated and the symmetry plane was orthogonal to the axis of the rotation. However, whether the flow was steady or unsteady depended on the Reynolds number and the rotational speed. At Re = 100, the flow was steady planar-symmetric for all the cases of $\omega^* > 0$. On the other hand, at Re = 250 and 300, the flows experienced a sequence of transitions between steady planar-symmetric and unsteady planar-symmetric flows with increasing ω^*.

One of the interesting issues is whether or not the rotation of the sphere can suppress vortex shedding from the sphere. To resolve this issue, the characteristics of vortex shedding were examined in detail. At Re = 300, vortex shedding occurred at low values of ω^* maintaining the form of hairpin vortices, but it was completely suppressed at $\omega^* = 0.4$ and 0.6. Interestingly, however, at $\omega^* = 1$ and 1.2, unsteady vortex loops were newly generated in the wake due to the shear layer instability. The two unsteady flow regimes, separated by the steady one, were very dif-

ferent in the vortex shedding frequency as well as vortical structures. The Strouhal number associated with the shear layer instability was much higher than that with vortex shedding of hairpin vortices. To the author's knowledge, this is the first attempt to report the suppression of vortex shedding from a sphere by the transverse rotation and the reappearance of unsteady flow due to the shear layer instability. In this study, it was not tried to find the exact boundary of ω^* at which vortex shedding is suppressed, but the upper boundary (critical rotational speed), over which the shear layer instability begins to appear, was shown to be higher at Re = 250 than at Re = 300. It was also shown that the time-averaged drag and lift coefficients monotonically increased with increasing rotational speed, agreeing well with the previous studies.

As explained so far, the effect of rotation on the flow is complicated for the entire range of ω^* investigated. However, if our attention is limited to the low rotational speed range ($\omega^* \le 0.25$), the effect of rotation can be summarized as follows: For the Reynolds number range considered, the slow rotation has a similar effect as increasing the Reynolds number. For example, the vortical structures behind a rotating sphere ($\omega^* = 0.25$) at Re = 100 and 250 were very similar to those behind a stationary sphere ($\omega^* = 0$) at Re = 250 and 300, respectively. Besides, increasing rotational speed ($0 \le \omega^* \le 0.25$) at Re = 300 had the same effect as increasing Reynolds number from Re = 300 without rotation ($\omega^* = 0$) in that both ways increase the vortex shedding frequency (see Fig. 14 and Sakamoto & Haniu [26]).

Acknowledgments

This work is supported by the Research Fund, Kumoh National Institute of Technology, and the support is gratefully acknowledged. Also, the author would like to express special thanks to Professor Haecheon Choi of Seoul National University for his helpful comments and discussions.

References

[1] H. Schlichting, *Boundary layer theory, McGraw-Hill*, New York, USA, (1979).

[2] S. Luthander and A. Rydberg, Experimentelle untersuchungen über den luftwiderstand bei einer um eine mit der windrichtung parallele achse rotierenden kugel, *Phys. Z*., 36 (1935) 552-558.

[3] N. E. Hoskin, The laminar boundary layer on a rotating sphere, *Fifty years of boundary layer research*, Braunschweig (1955) 127-131.

[4] D. Kim and H. Choi, Laminar flow past a sphere rotating in the streamwise direction, *J. Fluid Mech*., 461 (2002) 365-386.

[5] S. I. Rubinow and J. B. Keller, The transverse force on a spinning sphere moving in a viscous fluid, *J. Fluid Mech*., 11 (1961) 447-459.

[6] H. M. Barkla and L. J. Auchterlonie, The Magnus and Robins effect on rotating spheres, *J. Fluid Mech*., 47 (1971) 437-447.

[7] Y. Tsuji, Y. Morikawa and O. Mizuno, Experimental measurement of the Magnus force on a rotating sphere at low Reynolds numbers, *Trans. ASME: J. Fluids Eng*., 107 (1985) 484-488.

[8] B. Oesterlé and T. B. Dinh, Experiments on the lift of a spinning sphere in a range of intermediate Reynolds numbers, *Exp. Fluids*, 25 (1998) 16-22.

[9] R. Kurose and S. Komori, Drag and lift forces on a rotating sphere in a linear shear flow, *J. Fluid Mech*., 384 (1999) 183-206.

[10] H. Niazmand and M. Renksizbulut, Surface effects on transient three-dimensional flows around rotating spheres at moderate Reynolds numbers, *Computers & Fluids*, 32 (2003) 1405-1433.

[11] S. Kang, H. Choi and S. Lee, Laminar flow past a rotating circular cylinder, *Phys. Fluids*, 11 (11) (1999) 3312-3321.

[12] S. Mittal and B. Kumar, Flow past a rotating cylinder, *J. Fluid Mech*., 476 (2003) 303-334.

[13] D. Kim and H. Choi, Laminar flow past a rotating sphere in the transverse direction, 56th Annual Meeting of the Division of Fluid Dynamics, American Physical Society (2003).

[14] J. Kim, D. Kim and H. Choi, An immersed boundary finite-volume method for simulations of flow in complex geometries, *J. Comput. Phys*., 171 (2001) 132-150.

[15] D. Kim, H. Choi and H. Choi, Characteristics of laminar flow past a sphere in uniform shear, *Phys. Fluids*, 17 (2005) 103602-1-10.

[16] D. Kim and H. Choi, Laminar flow past a hemisphere, *Phys. Fluids*, 15 (8) (2003) 2457-2460.

[17] G. Yun, H. Choi and D. Kim, Turbulent flow past a sphere at Re = 3700 and 10^4, *Phys. Fluids*, 15 (2003) S6.

[18] G. Yun, D. Kim and H. Choi, Vortical structures behind a sphere at subcritical Reynolds numbers,

Phys. Fluids, 18 (2006) 015102-1-14.

[19] B. Fornberg, Steady viscous flow past a sphere at high Reynolds numbers, *J. Fluid Mech*., 190 (1988) 471-489.

[20] T. A. Johnson and V. C. Patel, Flow past a sphere up to a Reynolds number of 300, *J. Fluid Mech*., 378 (1999) 19-70.

[21] G. S. Constantinescu and K. D. Squires, LES and DES investigations of turbulent flow over a sphere, AIAA Paper 2000-0540 (2000).

[22] A. G. Tomboulides and S. A. Orszag, Numerical investigation of transitional and weak turbulent flow past a sphere, *J. Fluid Mech*., 416 (2000) 45-73.

[23] R. Mittal, A Fourier-Chebyshev spectral collocation method for simulating flow past spheres and spheroids, *Int. J. Numer. Meth. Fluids*, 30 (1999) 921-937.

[24] R. Mittal, Planar symmetry in the unsteady wake of a sphere, *AIAA J*., 37 (3) (1999) 388-390.

[25] J. Jeong and F. Hussain, On the identification of a vortex, *J. Fluid Mech*., 285 (1995) 69-94.

[26] H. Sakamoto and H. Haniu, A study on vortex shedding from spheres in a uniform flow, *Trans. ASME: J. Fluids Eng*., 112 (1990) 386-392.

Dongjoo Kim is an associate professor in the School of Mechanical Engineering at Kumoh National Institute of Technology. His research interests include computational fluid dynamics, bluff-body wakes, and control of turbulent flows. He has a PhD in mechanical engineering from Seoul National University. He is a member of the American Physical Society and the American Institute of Aeronautics and Astronautics.